

## Article

# First-Principles Investigation into the Interaction of H<sub>2</sub>O with $\alpha$ -CsPbI<sub>3</sub> and the Intrinsic Defects within It

Na Wang<sup>1,2,\*</sup> and Yaqiong Wu<sup>1,2</sup><sup>1</sup> Department of Physical Chemistry, University of Science and Technology Beijing, Beijing 100083, China<sup>2</sup> School of Metallurgical and Ecological Engineering, University of Science and Technology, Beijing 100083, China

\* Correspondence: nawang@ustb.edu.cn

**Abstract:** CsPbI<sub>3</sub> possesses three photoactive black phases ( $\alpha$ ,  $\beta$ , and  $\gamma$ ) with perovskite structures and a non-photoactive yellow phase ( $\delta$ ) without a perovskite structure. Among these,  $\alpha$ -CsPbI<sub>3</sub> exhibits the best performance. However, it only exists at high temperatures and it tends to transform into the  $\delta$  phase at room temperature, especially in humid environments. Therefore, the phase stability of CsPbI<sub>3</sub>, especially in humid environments, is the main obstacle to its further development. In this study, we studied the interaction of H<sub>2</sub>O with  $\alpha$ -CsPbI<sub>3</sub> and the intrinsic defects within it. It was found that the adsorption energy in the bulk is higher than that on the surface ( $-1.26$  eV in the bulk in comparison with  $-0.60$  eV on the surface); thus, H<sub>2</sub>O is expected to have a tendency to diffuse into the bulk once it adsorbs on the surface. Moreover, the intrinsic vacancy of V<sub>Pb</sub><sup>0</sup> in the bulk phase can greatly promote H<sub>2</sub>O insertion due to the rearrangement of two I atoms in the two PbI<sub>6</sub> octahedrons nearest to V<sub>Pb</sub><sup>0</sup> and the resultant breaking of the Pb–I bond, which could promote the phase transition of  $\alpha$ -CsPbI<sub>3</sub> in a humid environment. Moreover, H<sub>2</sub>O adsorption onto V<sub>I</sub><sup>+1</sup> contributes to a further distortion in the vicinity of V<sub>I</sub><sup>+1</sup>, which is expected to enhance the effect of V<sub>I</sub><sup>+1</sup> on the phase transition of  $\alpha$ -CsPbI<sub>3</sub>. Clarifying the interaction of H<sub>2</sub>O with  $\alpha$ -CsPbI<sub>3</sub> and the intrinsic defects within it may provide guidance for further improvements in the stability of  $\alpha$ -CsPbI<sub>3</sub>, especially in humid environments.

**Keywords:** CsPbI<sub>3</sub>; H<sub>2</sub>O; vacancy; binding energy; stability

**Citation:** Wang, N.; Wu, Y. First-Principles Investigation into the Interaction of H<sub>2</sub>O with  $\alpha$ -CsPbI<sub>3</sub> and the Intrinsic Defects within It. *Materials* **2024**, *17*, 1091. <https://doi.org/10.3390/ma17051091>

Academic Editor: Bryan M. Wong

Received: 20 November 2023

Revised: 3 February 2024

Accepted: 5 February 2024

Published: 27 February 2024



**Copyright:** © 2024 by the authors. Licensee MDPI, Basel, Switzerland. This article is an open access article distributed under the terms and conditions of the Creative Commons Attribution (CC BY) license (<https://creativecommons.org/licenses/by/4.0/>).

## 1. Introduction

Over the last decade, the efficiency of organic–inorganic hybrid halide perovskite (HHP) solar cells has improved, and now ranges from 3.8% to 25.2% [1–6]. However, HHP solar cells are generally less stable due to the volatility and hygroscopicity of organic cations in the perovskite light-collecting layer [7–9]. The low stability of typical HHPs, such as MAPbI<sub>3</sub> (MA<sup>+</sup>: methylammonium) and FAPbI<sub>3</sub> (FA<sup>+</sup>: formamidinium), has been noted since the early stages of perovskite solar cell (PSC) research [7–9]. In order to address the “vulnerability” of HHP in ambient air, organic components, including MA<sup>+</sup> and FA<sup>+</sup>, have been partially or even completely replaced by Cs<sup>+</sup> or Rb<sup>+</sup> [10–13]. Completely inorganic halide perovskites (IHPs) show greater prospects for photoelectric applications because of their suitable optical properties and higher stability under external stimuli [14]. Among these, CsPbI<sub>3</sub> is the most typical, with a lower production cost [13,15–18]. Furthermore, cubic  $\alpha$ -CsPbI<sub>3</sub> has a direct band gap [19], a wide absorption spectrum in the solar region, high quantum efficiency, and a long radiation life, meaning that it is expected to be an excellent candidate for use in perovskite solar cells [20]. However, three photoactive “black” perovskite phases ( $\alpha$ ,  $\beta$ , and  $\gamma$ ) of CsPbI<sub>3</sub> can be easily transformed into a more thermodynamically stable “yellow” non-perovskite phase ( $\delta$  phase) under ambient conditions [21,22], and this polymorphic transformation becomes even more severe when water is present [16,23].

Various theoretical studies have revealed the possible degradation mechanism of CsPbI<sub>3</sub> in a humid environment. The transformation of CsPbI<sub>3</sub> from the  $\alpha$  to  $\delta$  phases has always been attributed to the lower formation enthalpy of the  $\delta$  phase [16]. Moreover, the instability of the  $\alpha$  phase of CsPbI<sub>3</sub> has been well documented to be attributed to the phonon instability of  $\alpha$ -CsPbI<sub>3</sub> [24,25]. Kye et al. have further pointed out that the cation vacancy ( $V_{Cs}$  and  $V_{Pb}$ ) can weaken the interaction between Cs and PbI<sub>6</sub> and may lower the nucleation barrier, thus promoting phase transformation [26]. On the other hand, Lin et al. have pointed out that I vacancies ( $V_I$ ) could reduce the surface tension between the  $\alpha$  and  $\delta$  phases and lower the nucleation barrier [23]. It has also been preliminarily determined that H<sub>2</sub>O induces a catalytic effect [16]. Jiang et al. [27] studied the effects of several air molecules and found that H<sub>2</sub>O may diffuse into and produce a polycrystalline structure and grain boundary, and eventually lead to the phase transformation of CsPbI<sub>3</sub>. Li et al. [28] have explored the counterpart system, CsSnI<sub>3</sub>, and found that the strong coupling between O and Cs and the hydrogen bond between H and I may lead to the deformation of the (001) surface and, thus, phase instability. Moreover, Lin et al. have also further elaborated that H<sub>2</sub>O adsorbed on the surface of  $\alpha$ -CsPbI<sub>3</sub> film may introduce  $V_I$ , thus effectively catalyzing the transformation from the  $\alpha$  to  $\delta$  phases [23].

However, the exquisite interaction of H<sub>2</sub>O with CsPbI<sub>3</sub> and the intrinsic defects within it have not yet been studied. Based on first-principles calculations, we first compared the interaction of H<sub>2</sub>O on the (001) surface and in the bulk of  $\alpha$ -CsPbI<sub>3</sub>. It was found that H<sub>2</sub>O binds more strongly in bulk  $\alpha$ -CsPbI<sub>3</sub> than on the surface; thus, H<sub>2</sub>O tends to diffuse into the bulk. Moreover, we further analyzed the interaction between H<sub>2</sub>O and the neutral and charged intrinsic vacancies in  $\alpha$ -CsPbI<sub>3</sub>. It was found that a neutral Pb vacancy  $V_{Pb}^0$  may significantly accelerate the insertion of H<sub>2</sub>O. The strong binding between H<sub>2</sub>O and  $V_{Pb}^0$  induces Pb–I bond breakage and new I–I bond formation, which are expected to promote the phase transition. Moreover, H<sub>2</sub>O adsorption onto  $V_I^{+1}$  contributes to a further distortion in the vicinity of  $V_I^{+1}$ , which is expected to enhance the phase transition effect of  $V_I^{+1}$ . This work may provide guidance for the improved stability of CsPbI<sub>3</sub>.

## 2. Calculation

All the calculations were performed using the code of the Vienna ab initio simulation package (VASP) [29] within the density functional theory (DFT) framework [30]. The Perdew–Burke–Ernzerh (PBE) [29] exchange–correlation function within the generalized gradient approximation (GGA) [31] method was used, and the plane wave cutoff energy was 450 eV. The optimized lattice constants of the  $\alpha$ -CsPbI<sub>3</sub> structure (pm3m) were  $a = b = c = 6.414 \text{ \AA}$ , which are consistent with the previous calculations (6.40  $\text{\AA}$ ) and experimental measurements (6.18  $\text{\AA}$ ) [32,33]. All of the atoms were fully relaxed, until the total energy per atom was less than  $1 \times 10^{-6}$  eV and the Hellmann–Feynman force per atom was less than 0.01 eV/ $\text{\AA}$ . For adsorption on the  $\alpha$ -CsPbI<sub>3</sub> (001) surface systems, we expanded the unit cell into a  $2 \times 2$  supercell in the ab plane and selected a K-mesh size of  $3 \times 3 \times 1$ ; for the insertion of H<sub>2</sub>O into the bulk phase of  $\alpha$ -CsPbI<sub>3</sub>, we constructed a  $3 \times 3 \times 3$  supercell and used a  $2 \times 2 \times 2$  Monkhorst–Pack K-mesh. We chose the CsI-terminated CsPbI<sub>3</sub> (001) surface because this is the most stable surface with the lowest surface energy, as examined in [34]. A vacuum layer of 18  $\text{\AA}$  was added in the (001) direction for the surface calculations in order to avoid interactions between the layers. For H<sub>2</sub>O adsorption and insertion into  $\alpha$ -CsPbI<sub>3</sub>, the structures were optimized, the internal coordinates fully relaxed, and the lattice parameters fixed. As far as the van der Waals (vdW) forces are concerned, we conducted D3 dispersion correction [35] for the pristine  $\alpha$ -CsPbI<sub>3</sub>. The lattice constant was reduced by 0.09  $\text{\AA}$ , which represents a decrease of around 1.4%. Considering that D3 dispersion correction would increase the binding energy between H and I, which may compensate for the lattice constant reduction, the conclusions drawn in our work are not expected to be affected. Because Cs, Pb, and I are heavy, spin–orbit coupling (SOC) [36] may be significant. As Li et al. [33] have found, SOC mainly decreases the conduction band. Furthermore, it has been found that a GW [37] + SOC calculation can increase the band gap

back close to the PBE results. Thus, it seems PBE calculation provides reasonable results for the numerical compensation between GW and SOC.

### 3. Results and Discussion

The instability of CsPbI<sub>3</sub> with a highly symmetrical perovskite structure is mainly due to the size mismatch between the constituent ions. In order to stabilize the small Cs in the PbI<sub>6</sub> octahedral gap, the PbI<sub>6</sub> octahedron rotates and tilts, resulting in the distortion of the highly symmetrical perovskite structure so as to form less symmetrical non-perovskite structures. Thus, though it possesses better photoelectric properties [19], the cubic structure of CsPbI<sub>3</sub> is very unstable, and recent experiments and calculations have focused on the instability of  $\alpha$ -CsPbI<sub>3</sub>. Therefore, in this work, we focused mainly on the interaction of H<sub>2</sub>O with pristine  $\alpha$ -CsPbI<sub>3</sub> and the intrinsic defects within it. The  $\alpha$ - and  $\delta$ -CsPbI<sub>3</sub> structures are shown in Figure 1. PbI<sub>6</sub> extends its three-dimensional framework in an angle-sharing manner along the three coordinate axis directions in  $\alpha$ -CsPbI<sub>3</sub>, with a Cs atom in the middle of the eight top corners, a Pb atom in the center of the cubic structure, and an I atom in the six faces of the cube center. PbI<sub>6</sub> rotates and breaks into  $\delta$ -CsPbI<sub>3</sub>. As shown, the  $\alpha$ -to- $\delta$ -CsPbI<sub>3</sub> phase transition involves bond breaking and rebonding [38]. However, the bond rearrangement barrier may be high in the pristine lattice and so the intrinsic defects are expected to play a role in phase transformation [23,26]. H<sub>2</sub>O,  $\alpha$ -CsPbI<sub>3</sub>, and the intrinsic defects may also interact.

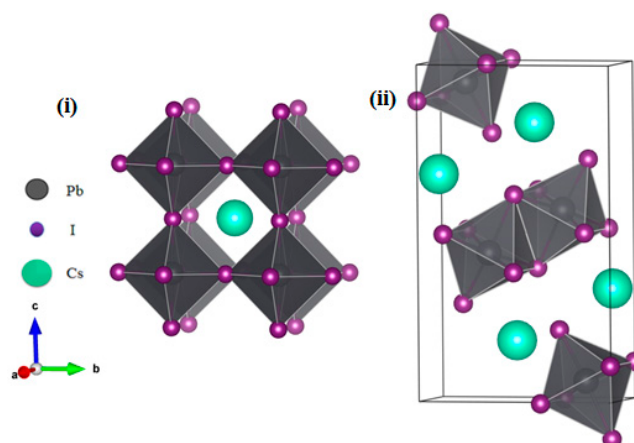


**Figure 1.** The unit cell structure of  $\alpha$ -CsPbI<sub>3</sub> (i) and  $\delta$ -CsPbI<sub>3</sub> (ii). The Cs, Pb, and I ions are shown as large green, gray, and small purple circles, respectively. The lattice vectors are labeled as a, b, c in (i).

#### 3.1. Comparison of Adsorption of H<sub>2</sub>O on the Surface and in the Bulk of CsPbI<sub>3</sub>

Regarding the position of H<sub>2</sub>O in CsPbI<sub>3</sub>, we first calculated the binding energy  $E_{\text{bind}}$  of H<sub>2</sub>O on the surface and in the bulk of  $\alpha$ -CsPbI<sub>3</sub>. Figure 2 shows the structures of the bulk and (001) surface of  $\alpha$ -CsPbI<sub>3</sub> with and without H<sub>2</sub>O adsorption. For H<sub>2</sub>O insertion into the  $\alpha$ -CsPbI<sub>3</sub> bulk, the H<sub>2</sub>O molecule was placed into three different positions, ensuring that O was close to the Cs and that H was close to the I atoms; however, the optimized structure of the three different initial configurations became similar as a result of O binding with Cs and two H atoms binding with I, as can be seen in Figure 2b. The distance between Cs and O is 2.92 Å, and the distance between the two H and I atoms are around 2.65 Å. The binding energy of the three configurations are also similar, as can be seen in Table 1. For H<sub>2</sub>O adsorption on the surface, we first generated the possible configurations that could favor Cs–O and I–H bonds, referencing the configurations in [28]. Similar to this study, the energy difference between the different configurations is small, and we show one of the configurations in Figure 2d. The distance between Cs and O is 3.04 Å, which is a little larger than that in the bulk, and the distance between H and I is around 2.60 Å, which is a little smaller than that in the bulk. The strong coupling between O and Cs and the interaction

between H and I led to the strong binding of H<sub>2</sub>O in CsPbI<sub>3</sub>, as in CsSnI<sub>3</sub> [28]. The binding energy of H<sub>2</sub>O in the bulk and on the surface of  $\alpha$ -CsPbI<sub>3</sub> can be calculated as follows:

$$E_{\text{bind}} = E_{\text{ads}} - E_{\text{noH}_2\text{O}} - E_{\text{H}_2\text{O}} \quad (1)$$

where  $E_{\text{bind}}$  represents the binding energy,  $E_{\text{ads}}$  and  $E_{\text{noH}_2\text{O}}$  represent the total energies of the bulk or surface system with and without H<sub>2</sub>O adsorbed, respectively, and  $E_{\text{H}_2\text{O}}$  is the total energy of one H<sub>2</sub>O molecule. The energy of the H<sub>2</sub>O molecule was calculated within a cell with a vacuum size of 10 Å to ensure the H<sub>2</sub>O molecule fully separated from its periodic images. The binding energies of H<sub>2</sub>O in the bulk and on the surface of  $\alpha$ -CsPbI<sub>3</sub> are both negative, −1.26 eV and −0.60 eV, respectively, indicating that the binding process is exothermic and can proceed spontaneously, in accordance with prior research on CsSnI<sub>3</sub>. The binding energy is higher in the bulk than that on the surface, even though H<sub>2</sub>O insertion into the bulk may cause a larger distortion, and this could be indicative of the instability of CsPbI<sub>3</sub>, and, thus, CsPbI<sub>3</sub> could potentially bond with H<sub>2</sub>O. In this regard, H<sub>2</sub>O tends to diffuse into the bulk once it adsorbs on the surface. Thus, we focused on the interaction between H<sub>2</sub>O and the intrinsic defects in the  $\alpha$ -CsPbI<sub>3</sub> bulk in this work.

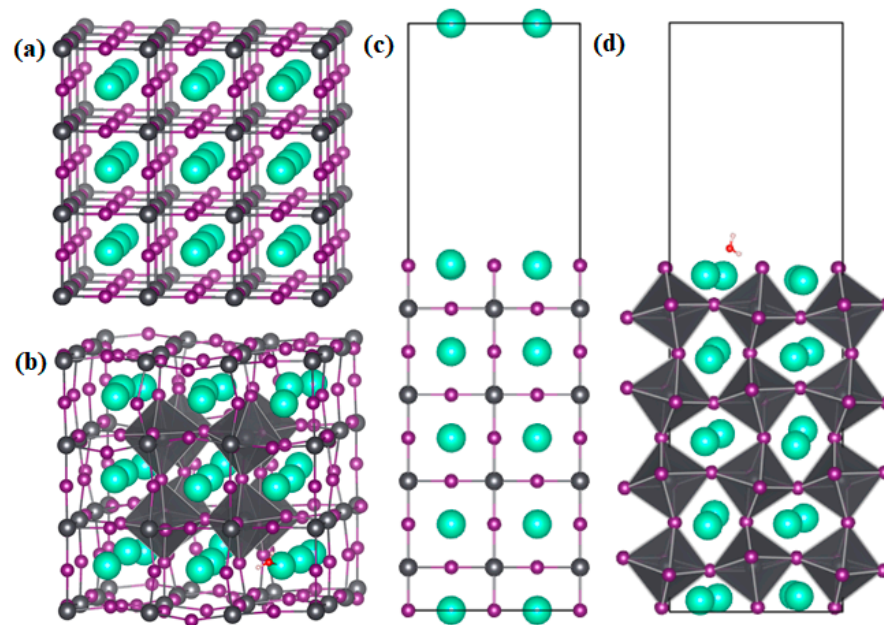


**Figure 2.** Structures of (a,b) bulk and (c,d) (001) surface of  $\alpha$ -CsPbI<sub>3</sub> with and without H<sub>2</sub>O adsorption. The Cs, Pb, and I ions are shown as large green, gray, and small purple circles, respectively. O and H are shown as small red and white circles.

**Table 1.** Binding energy of H<sub>2</sub>O in the bulk of  $\alpha$ -CsPbI<sub>3</sub> at different initial positions.

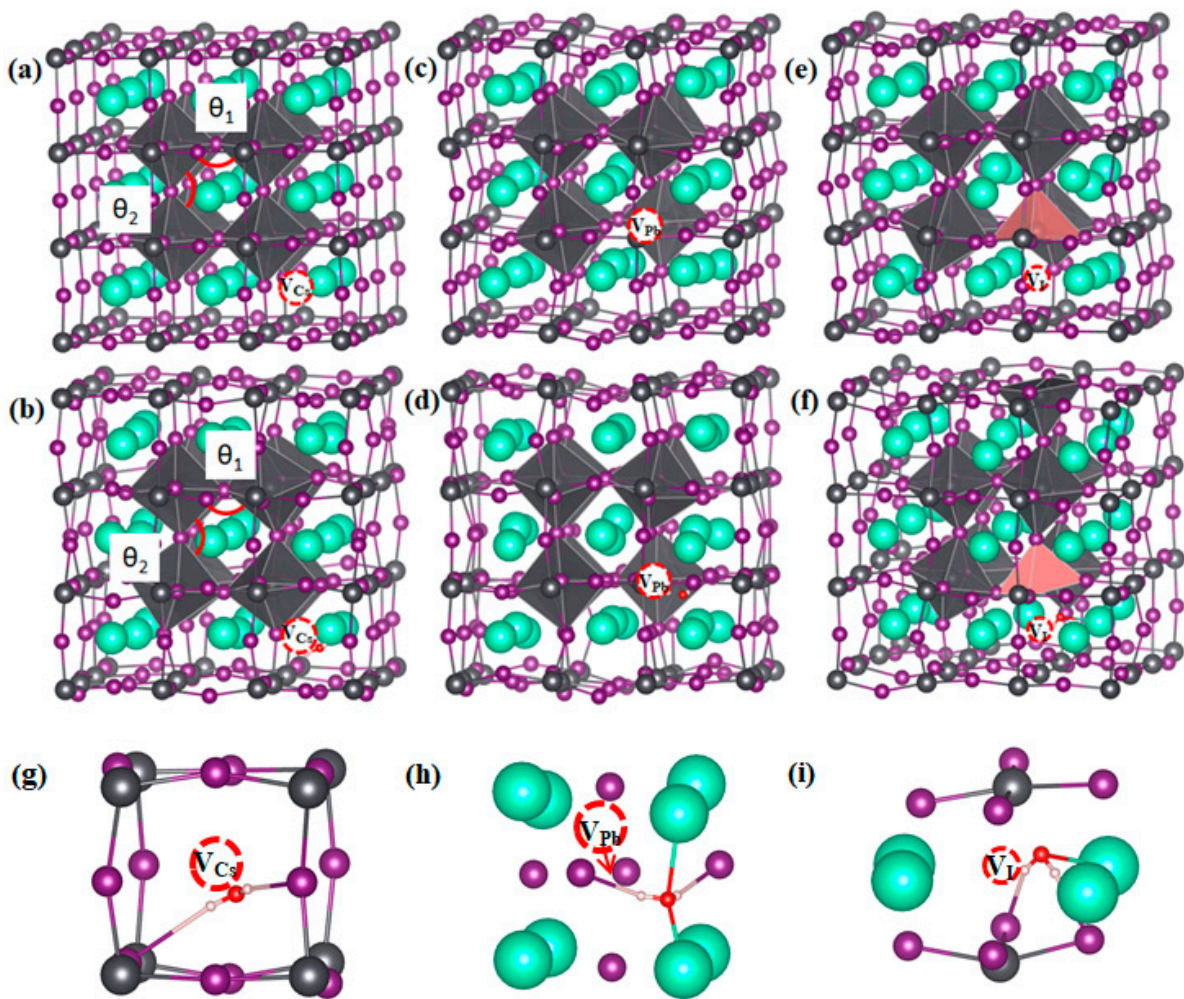
| Initial Position of H <sub>2</sub> O Insertion | Binding Energy $E_{\text{bind}}$ /eV |
|--|--------------------------------------|
| near Cs  | −1.21                                |
| near Pb  | −1.25                                |
| near I   | −1.26                                |

### 3.2. Effect of Intrinsic Vacancies within the Bulk Phase on H<sub>2</sub>O Insertion

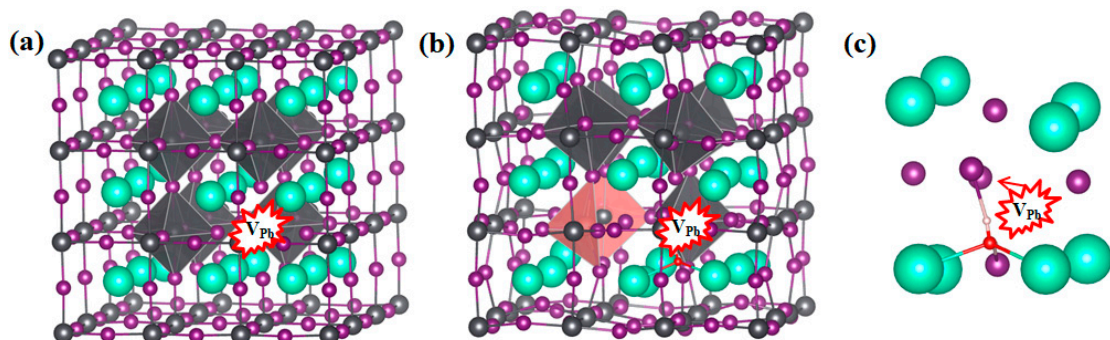
The distribution of the intrinsic defects can usually be estimated with the concentration formula  $c = N_{\text{sites}} e^{-\Delta H/kT}$ , where  $c$  represents the concentration of the defect,  $N_{\text{sites}}$  represents the number of sites for the defect per unit volume,  $\Delta H$  represents the formation energy of the defect, and  $k$  and  $T$  represent the Boltzmann constant and temperature, respectively [39]. The formation energies depend on the chemical potentials of the constituent element. As Li et al. [33,40] have calculated, there could be different intrinsic defects within

the CsPbI<sub>3</sub> bulk phase, and they found that the formation energies of Pb, the I vacancy  $V_{\text{Pb}}$ , and  $V_{\text{I}}$  are extremely low, and even negative, under both Pb/Cs-rich and I-rich conditions. The formation energy of Cs vacancy,  $V_{\text{Cs}}$ , is also relatively low. Thus, the dominant defects in  $\alpha$ -CsPbI<sub>3</sub> are  $V_{\text{Pb}}$ ,  $V_{\text{Cs}}$ , and  $V_{\text{I}}$ ; moreover,  $V_{\text{Pb}}$  and  $V_{\text{Cs}}$  tend to be negatively charged  $V_{\text{Cs}}^{-1}$  and  $V_{\text{Pb}}^{-2}$ , respectively, while  $V_{\text{I}}$  tends to be positively charged  $V_{\text{I}}^{+1}$ . Thus, based on a previous study, we studied the interaction of H<sub>2</sub>O with three intrinsic vacancies,  $V_{\text{Cs}}$ ,  $V_{\text{Pb}}$ , and  $V_{\text{I}}$ , in  $\alpha$ -CsPbI<sub>3</sub> bulk, and the neutral,  $V_{\text{Cs}}^0$ ,  $V_{\text{Pb}}^0$ , and  $V_{\text{I}}^0$ , and charged states,  $V_{\text{Cs}}^{-1}$ ,  $V_{\text{Pb}}^{-2}$ , and  $V_{\text{I}}^{+1}$  [33], were both studied. H<sub>2</sub>O was inserted close to the vacancies, and the relative position for H<sub>2</sub>O with respect to the vacancies can be seen in Figures 3 and 4. The structures given were optimized. The binding energies for H<sub>2</sub>O close to the vacancies can also be calculated with Equation (1), and the results can be seen in Table 2. The long-range Coulomb interactions converge slowly with the supercell size; thus, charge–charge corrections are sometimes needed [39]. We addressed the energy difference before and after H<sub>2</sub>O insertion and, thus, the electrostatic energy from the spuriously repeated charges was expected to be canceled out. Moreover, this process has not been conducted when calculating the  $3 \times 3 \times 3$  supercells of  $\alpha$ -CsPbI<sub>3</sub> [33]. Therefore, charge–charge correction was neglected in this work. As shown, and compared with that in the pristine lattice, the binding energy of H<sub>2</sub>O near the charged vacancies,  $V_{\text{Cs}}^{-1}$ ,  $V_{\text{I}}^{+1}$ , and  $V_{\text{Pb}}^{-2}$ , decreased or was almost unchanged. The binding energy of H<sub>2</sub>O near the neutral vacancies,  $V_{\text{I}}^0$  and  $V_{\text{Cs}}^0$ , further decreased, which could be attributed to the decreased charge on the atoms near  $V_{\text{I}}^0$  and  $V_{\text{Cs}}^0$ , which in turn reduced the Coulomb attraction between I/Cs and H<sub>2</sub>O, which were responsible for the binding between H<sub>2</sub>O and CsPbI<sub>3</sub> [28]. However, the introduction of  $V_{\text{Pb}}^0$  significantly increased the binding energy of H<sub>2</sub>O. We then analyzed the changes in the structures in these systems. It must be noted that no matter which vacancy was introduced, the insertion energy was always negative, indicating that the insertion of H<sub>2</sub>O is always an exothermic process and can spontaneously occur.

Figure 3 shows the optimized structure of  $\alpha$ -CsPbI<sub>3</sub> with  $V_{\text{Cs}}^{-1}$ ,  $V_{\text{I}}^{+1}$ , and  $V_{\text{Pb}}^{-2}$  with or without H<sub>2</sub>O inserted. As shown, when only  $V_{\text{Cs}}^{-1}$  or  $V_{\text{Pb}}^{-2}$  was introduced, the original cubic structure was not significantly distorted, and the octahedron did not significantly rotate or twist. In the vicinity of the  $V_{\text{Cs}}^{-1}$  vacancy, due to the removal of the attraction of Cs, I slightly moved away from the vacancy, the nearest Pb–I bond was slightly bent, and the remaining I atoms and all of the Pb and Cs atoms are located in their original highly symmetrical position without being offset. For  $V_{\text{Pb}}^{-2}$ , compared with the perfect supercell, the bond length of I–Pb adjacent to  $V_{\text{Pb}}^{-2}$  was reduced by about 0.1 Å; however, the I–Pb–I bond angle was basically unchanged. Thus, the octahedron framework did not deviate from the perfect supercell, and only adjacent Cs was slightly shifted towards  $V_{\text{Pb}}^{-2}$ . However, when  $V_{\text{I}}^{+1}$  was introduced, the PbI<sub>6</sub> octahedron rotated and twisted to a large extent, and Cs also deviated from the center and moved away from  $V_{\text{I}}^{+1}$ , due to the removal of the attraction or repulsion of the I. The large distortion induced by  $V_{\text{I}}^{+1}$  is consistent with the results of Lin et al. [23], who found that  $V_{\text{I}}^{+1}$  in the crystal lattice can effectively catalyze the transformation from the  $\alpha$  to  $\delta$  phases. However, when H<sub>2</sub>O is introduced to  $V_{\text{Cs}}^{-1}$  and  $V_{\text{Pb}}^{-2}$ , the structures in the vicinity of the vacancies become significantly distorted. Moreover, H<sub>2</sub>O adsorption onto  $V_{\text{I}}^{+1}$  contributes to further distortion in the vicinity of  $V_{\text{I}}^{+1}$ , thus enhancing its effect on phase transformation. To manifest the rotation or twisting of the octahedron, we measured the 2 I–I–I bond angles between the octahedrons close to the vacancies,  $\theta_1$  and  $\theta_2$ , as labeled in Figure 3, and the results are shown in Figure 5. As shown,  $\theta_1$  and  $\theta_2$  were almost 90° when only  $V_{\text{Cs}}^{-1}$  or  $V_{\text{Pb}}^{-2}$  was introduced, and they shifted away from 90° when only  $V_{\text{I}}^{+1}$  was introduced. Additionally,  $\theta_1$  and  $\theta_2$  shifted away from 90° when H<sub>2</sub>O was then introduced to  $V_{\text{Cs}}^{-1}$  or  $V_{\text{Pb}}^{-2}$ , even though this shift is still smaller than that for only  $V_{\text{I}}^{+1}$ . Another shift occurred on  $\theta_1$  and  $\theta_2$  when H<sub>2</sub>O was further introduced to  $V_{\text{I}}^{+1}$ , indicating that H<sub>2</sub>O adsorption onto  $V_{\text{I}}^{+1}$  further contributes to the effect of  $V_{\text{I}}^{+1}$  on the phase transition of CsPbI<sub>3</sub>.



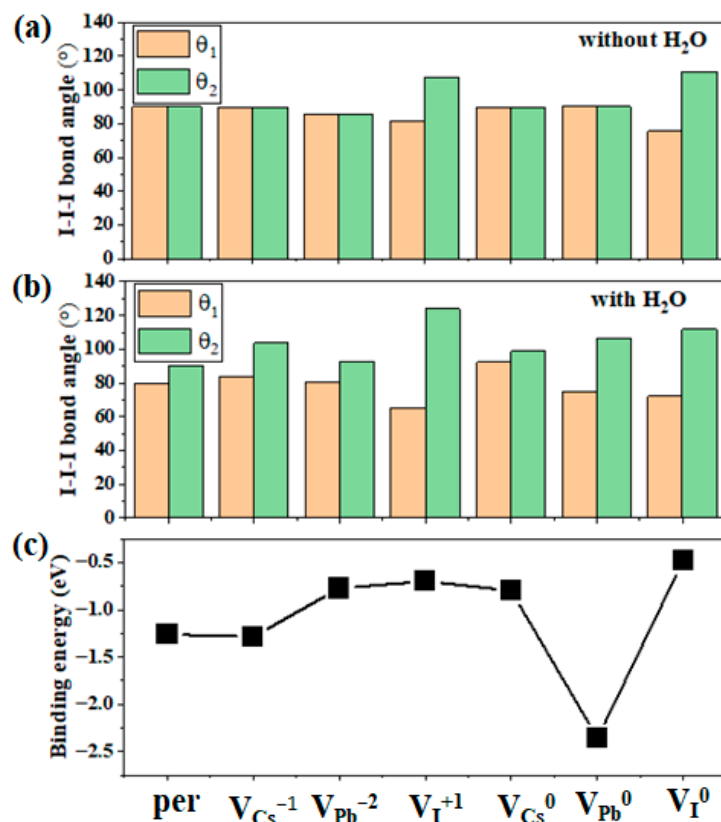
**Figure 3.** Structures of  $\text{CsPbI}_3$  in the  $3 \times 3 \times 3$  supercells (40 atoms) with Cs, I, and Pb vacancies,  $V_{\text{Cs}}^{-1}$ ,  $V_{\text{I}}^{+1}$ , and  $V_{\text{Pb}}^{-2}$  (a,c,e), without and (b,d,f) with  $\text{H}_2\text{O}$  inserted. The enlarged parts around the vacancies with  $\text{H}_2\text{O}$  inserted are shown in (g–i).  $\theta_1$  and  $\theta_2$  represent the 2 I–I–I bond angles between octahedrons close to the vacancies. The atom colors adopted are the same as those in Figure 1. The  $\text{PbI}_6$  octahedron is marked in gray, and the  $\text{PbI}_5$  octahedron is marked in pink. The positions for  $V_{\text{Cs}}^{-1}$ ,  $V_{\text{I}}^{+1}$ , and  $V_{\text{Pb}}^{-2}$  are surrounded by a dashed circle.



**Figure 4.** Structures of  $\text{CsPbI}_3$  in the  $3 \times 3 \times 3$  supercells (40 atoms) with the Cs, I, and Pb vacancies,  $V_{\text{Pb}}^0$ , (a) without and (b) with  $\text{H}_2\text{O}$  inserted. The enlarged parts around the vacancies with  $\text{H}_2\text{O}$  inserted are shown in (c). The atom and  $\text{PbI}_6$  octahedron colors adopted are the same as those in Figure 3. The positions for  $V_{\text{Pb}}^{-2}$  are surrounded by a red shape.

**Table 2.** Binding energy of H<sub>2</sub>O near different vacancies in the bulk of  $\alpha$ -CsPbI<sub>3</sub>.

| Position of H <sub>2</sub> O Insertion | Binding Energy $E_{\text{bind}}/\text{eV}$ |
|--|--|
| Near $V_{\text{Cs}}^{-1}$              | −1.29                                      |
| Near $V_{\text{Pb}}^{-2}$              | −0.78                                      |
| Near $V_{\text{I}}^{+1}$               | −0.70                                      |
| Near $V_{\text{Cs}}^0$                 | −0.80                                      |
| Near $V_{\text{Pb}}^0$                 | −2.36                                      |
| Near $V_{\text{I}}^0$                  | −0.48                                      |

**Figure 5.** I–I bond angles  $\theta_1$  and  $\theta_2$  between octahedrons close to the position of H<sub>2</sub>O, as marked in Figure 3, (a) before and (b) after H<sub>2</sub>O insertion. (c) Binding energies for H<sub>2</sub>O in CsPbI<sub>3</sub>, including the vacancies and the pristine lattice.

On the other hand, for the neutral state, the distortion induced by H<sub>2</sub>O adsorption onto  $V_{\text{Cs}}^0$  and  $V_{\text{I}}^0$  is smaller compared with their charged states, while the distortion induced by H<sub>2</sub>O adsorption onto  $V_{\text{Pb}}^0$  is larger, which is in accordance with the insertion energy trend. Thus, we focused on the effect of H<sub>2</sub>O adsorption onto  $V_{\text{Pb}}^0$ . Figure 4 shows the optimized structures of  $V_{\text{Pb}}^0$  before and after inserting H<sub>2</sub>O near  $V_{\text{Pb}}^0$ . As shown, when we introduced only  $V_{\text{Pb}}^0$  to  $\alpha$ -CsPbI<sub>3</sub>, the symmetrical structure of  $\alpha$ -CsPbI<sub>3</sub> remained basically unchanged. However, when we inserted H<sub>2</sub>O near  $V_{\text{Pb}}^0$ , a huge distortion of the structure was induced, and this distortion is even comparable with the distortion induced by  $V_{\text{I}}^-$ . An important feature is that some of the PbI<sub>6</sub> octahedrons actually “disintegrated”, with the measured distances between Pb and I increasing from 3.21 Å to 3.9 Å and 3.1 Å to 4.06 Å, respectively, and the two I atoms actually formed new I–I bonds. The Pb–I bond broke, and a new stable I–I bond formation may be the dominant reason for the significantly high binding energy for H<sub>2</sub>O inserted near  $V_{\text{Pb}}^0$ . To absolutely characterize the bonding nature for H<sub>2</sub>O near  $V_{\text{Pb}}^0$ , we conducted band structure and charge density calculations, as can be seen in Figure 6. We found that, as shown in Figure 6a, an isolated energy level formed, and that the corresponding charge was indeed located between the I atoms, as seen

in Figure 6b,c. The disintegrated  $\text{PbI}_6$  octahedrons and new I–I bond formation indicate that the effect of  $\text{H}_2\text{O}$  on  $V_{\text{Pb}}^0$  could equivalently be recognized as formation of two I vacancies,  $V_{\text{I}}$ , close to the one Pb vacancy,  $V_{\text{Pb}}$ . The large distortion induced is consistent with the effect of the  $V_{\text{I}}$  vacancies and, thus, may also promote  $\alpha$ -to- $\delta$ -phase transformation. In addition, the binding energy of  $\text{H}_2\text{O}$  near  $V_{\text{Pb}}^0$  is around 2 eV higher than that of  $V_{\text{Pb}}^{2-}$ , and the formation energy of  $V_{\text{Pb}}^{2-}$  is only nearly 2 eV lower than that of  $V_{\text{Pb}}^0$  near the Fermi level, as can be found in [33]; thus,  $V_{\text{Pb}}^{2-}$  probably causes the transformation from  $V_{\text{Pb}}^{2-}$  to  $V_{\text{Pb}}^0$  and binds strongly with  $\text{H}_2\text{O}$  if  $\text{H}_2\text{O}$  is inserted. Considering its abundance, the transformation from  $V_{\text{Pb}}^{2-}$  to  $V_{\text{Pb}}^0$  and the strong binding with  $\text{H}_2\text{O}$  are expected to cause  $\text{H}_2\text{O}$  to catalyze the  $\alpha$ -to- $\delta$  phase transformation of  $\text{CsPbI}_3$ .

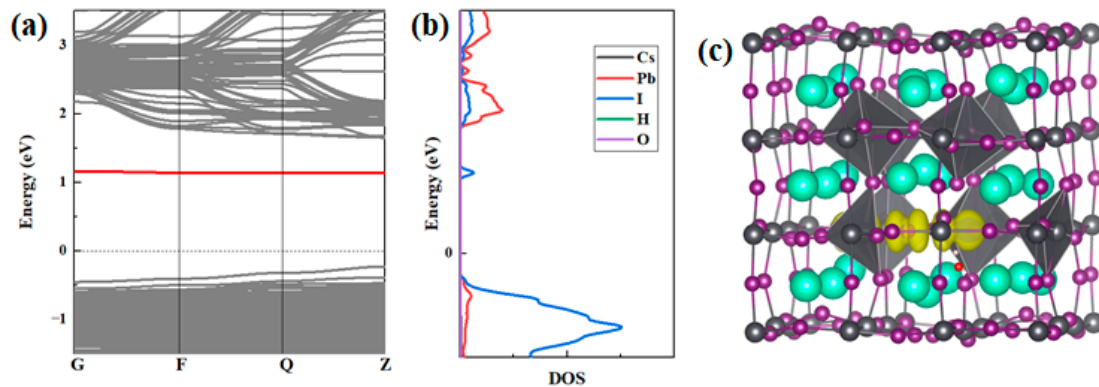


**Figure 6.** (a) The band structure and (b) the projected density of state (PDOS) for  $\text{CsPbI}_3$  in the  $3 \times 3 \times 3$  supercells (40 atoms) with neutral Pb vacancies  $V_{\text{Pb}}^0$ , with  $\text{H}_2\text{O}$  inserted. The defect level in (a) in the band gap is shown in red. The PDOSs for Cs, Pb, I, H, and O are given in different colors in (b). (c) The partial charge densities of the defect levels are shown in red (a). The atom colors adopted are the same as in Figure 1. The isosurface of the partial charge density is shown in yellow.

To further illustrate the interaction between the defects and  $\text{H}_2\text{O}$ , we calculated the formation energies of  $V_{\text{Cs}}$ ,  $V_{\text{Pb}}$ , and  $V_{\text{I}}$  in  $\alpha$ - $\text{CsPbI}_3$  with and without  $\text{H}_2\text{O}$  insertion, as shown in Figure 7. The formation energy is calculated with the following equation [39,41–45]:

$$\Delta H_f(q) = E(q) - E(\text{pristine}) + \sum_i n_i [\mu_i + E(i)] + q[E_F + \varepsilon_{\text{VBM}}] \quad (2)$$

where  $E(q)$  represents the energy of the defect system in charged state  $q$ ,  $E(\text{pristine})$  represents the energy of the pristine system,  $\varepsilon_{\text{VBM}}$  represents the energy of the valence band maximum (VBM), and  $E_F$  represents the Fermi energy in reference to  $\varepsilon_{\text{VBM}}$ .  $n_i$  represents the number of atoms  $i$  added ( $n_i < 0$ ) or removed ( $n_i > 0$ ) from the system,  $E(i)$  represents the energy of the element solid  $i$ , and  $\mu_i$  represents the chemical potential in reference to  $E(i)$ . The choice of  $E(i)$  for Cs, Pb, and I were the same as those in [33,40], and the  $E(i)$  for  $\text{H}_2\text{O}$  represents the energy of one  $\text{H}_2\text{O}$  molecule.

As shown, the formation energies of the defects without  $\text{H}_2\text{O}$  insertion are generally consistent with those in [33]. We compared the formation energies with and without  $\text{H}_2\text{O}$  insertion. As shown,  $\text{H}_2\text{O}$  insertion reduces the formation energy of the defects due to binding between  $\text{H}_2\text{O}$  and the different defects. Specifically, the formation energy of  $V_{\text{Pb}}^0$  could become lower than that for  $V_{\text{Pb}}^{2-}$  when the Fermi energy is near the VBM, and this is in accordance with the estimation we derived from binding energy analysis, in which  $V_{\text{Pb}}^{2-}$  is able to transform into  $V_{\text{Pb}}^0$ . Regarding the large deformation promoted in  $V_{\text{Pb}}^0$ , the formation of  $V_{\text{Pb}}^0$  is expected to be capable of promoting phase transition. Moreover, the formation of  $V_{\text{Pb}}^0$  tends to occur close to the VBM; the p-type samples synthesized under low-Pb-level conditions are expected to be affected more. We estimated the effect of charge–charge correction [42,44,45]. The charge–charge interaction between the periodic images could be estimated in the form  $\sim q^2/4\pi\epsilon L$  [46], where  $q$  represents the charge on the defect,  $L$  represents the lateral size of the supercell, and  $\epsilon$  represents the relative static

dielectric constant, which is around six in  $\alpha$ -CsPbI<sub>3</sub> [47]. We took  $V_{\text{Pb}}^{2-}$  with the higher valence of  $-2$  for the estimation, and the interaction energy is around 0.2 eV within the  $3 \times 3 \times 3$  supercell. This correction may move the  $0/-2$  transition level of  $V_{\text{Pb}}$  by around 0.1 eV; however, the main conclusions state that  $V_{\text{Pb}}^{2-}$  can transform into  $V_{\text{Pb}}^0$  when the Fermi energy located near the VBM does not change. On the other hand, we mainly compared the formation energy of the defects before and after H<sub>2</sub>O insertion in this work; the electrostatic energies from the spuriously repeated charges were expected to be canceled out. Moreover, regarding the defect levels of  $V_{\text{Pb}}$  that reside within the band gap between the unoccupied conduction bands, the main conclusion in this work is expected to be unaffected by the band filling effect [48].

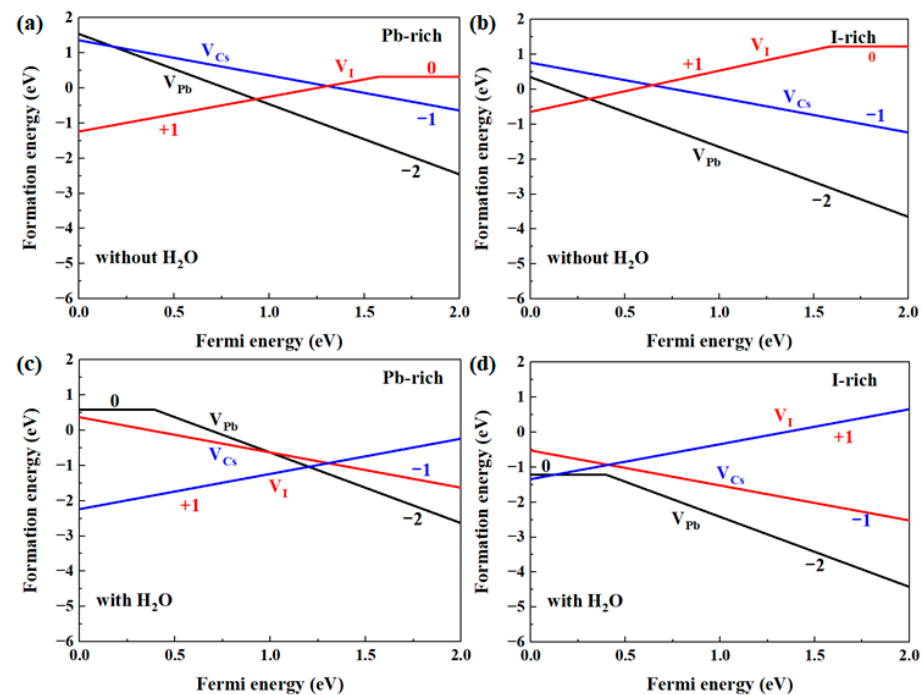


**Figure 7.** Formation energies of  $V_{\text{Pb}}$ ,  $V_{\text{Cs}}$ , and  $V_{\text{I}}$  in  $\alpha$ -CsPbI<sub>3</sub> at high- and low-Pb-level conditions (a,b) without and (c,d) with H<sub>2</sub>O. The charges on the defects are labeled alongside each segment.

It must be noted that polymorphous symmetry breaking may occur in  $\alpha$ -CsPbI<sub>3</sub>, where  $\alpha$ -CsPbI<sub>3</sub> possesses a polymorphous network arranged with local structural motifs of the low-temperature phase with low-level symmetry [24,49]. However, the dominant defects in the low-temperature  $\beta$ - or  $\gamma$ -CsPbI<sub>3</sub> are also  $V_{\text{Pb}}$ ,  $V_{\text{I}}$ , and  $V_{\text{Cs}}$ , as calculated in the previous literature [32]; thus, the defects that we chose to study in this work are reasonable. We conducted further calculations to explore the effect on the defect formation energy. In this work, we found that the dominant role that the defects may play in phase transition when H<sub>2</sub>O is present is that H<sub>2</sub>O can promote both the rearrangement of I atoms into PbI<sub>6</sub> octahedrons and the Pb–I bond breakage nearest to  $V_{\text{Pb}}^0$ , which can eventually promote phase transition. We then conducted a calculation for H<sub>2</sub>O insertion into  $V_{\text{Pb}}^0$  in  $\gamma$ -CsPbI<sub>3</sub>. However, as can be seen in Figure 8, no significant bond breakage or I atom rearrangements were found. This indicates that whether  $V_{\text{Pb}}^0$  takes effect indeed depends on the surrounding structures, and that limited deformation can occur in the low-level symmetry system, which is consistent with its higher stability. However, the cubic structure can possess more local deformations [24], revealing its higher flexibility. As a result, this depends on whether  $V_{\text{Pb}}^0$  in the cubic phase with local deformation can be deformed by H<sub>2</sub>O insertion. Moreover, there may be fluctuation in the local environment of  $V_{\text{Pb}}^0$  in the cubic phase, which may deserve further study.

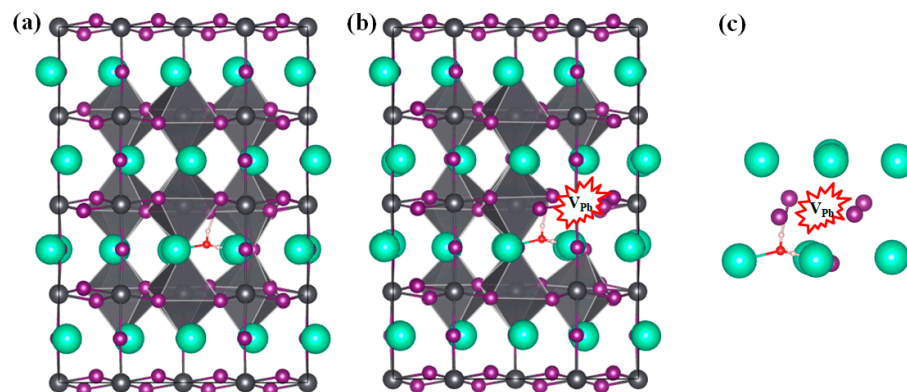


**Figure 8.** Structures of  $\gamma$ -CsPbI<sub>3</sub> (a) without and (b) with Pb vacancy  $V_{\text{Pb}}^0$ , and with H<sub>2</sub>O inserted. The enlarged parts around the vacancy with H<sub>2</sub>O inserted are shown in (c). The atom and PbI<sub>6</sub> octahedron colors adopted are the same as those in Figure 3. The positions for  $V_{\text{Pb}}^{-2}$  are surrounded by a red shape.

#### 4. Conclusions

In this paper, first-principles calculations based on the density functional theory are used to theoretically study the interaction between H<sub>2</sub>O and CsPbI<sub>3</sub>, including the pristine lattice and intrinsic vacancies therein, and the  $\alpha$ -to- $\delta$  phase transition of CsPbI<sub>3</sub> catalyzed by H<sub>2</sub>O is analyzed. First, we compared the binding of H<sub>2</sub>O on the surface and in the bulk of  $\alpha$ -CsPbI<sub>3</sub>, and the binding energy is higher in the bulk than it is on the surface, at  $-1.26$  and  $-0.60$  eV, respectively. Thus, H<sub>2</sub>O tends to diffuse into the bulk once it adsorbs on the surface. We further studied the interaction between three intrinsic vacancies,  $V_{\text{Pb}}$ ,  $V_{\text{I}}$ , and  $V_{\text{Cs}}$ , in the  $\alpha$ -CsPbI<sub>3</sub> bulk and H<sub>2</sub>O insertion. It was found that the insertion energy of H<sub>2</sub>O decreased or was almost unchanged upon the insertion of the charged vacancies,  $V_{\text{Cs}}^{-1}$ ,  $V_{\text{I}}^{+1}$ , and  $V_{\text{Pb}}^{-2}$ , and neutral vacancies,  $V_{\text{I}}^0$  and  $V_{\text{Cs}}^0$ , while the introduction of  $V_{\text{Pb}}^0$  significantly increased the binding energy of H<sub>2</sub>O and, thus, promoted the insertion of H<sub>2</sub>O into the lattice. The strong binding between H<sub>2</sub>O and  $V_{\text{Pb}}^0$  induced Pb–I bond breakage and new I–I bond formation, which are expected to play roles in the phase transition from  $\alpha$ -CsPbI<sub>3</sub> to  $\delta$ -CsPbI<sub>3</sub>. Moreover, H<sub>2</sub>O adsorption onto  $V_{\text{I}}^{+1}$  contributes to a larger distortion in the vicinity of  $V_{\text{I}}^{+1}$ , which is expected to enhance the phase transition effect of  $V_{\text{I}}^{+1}$ . The result is expected to provide guidance for the improvement of the stability of  $\alpha$ -CsPbI<sub>3</sub>, especially in humid environments.

**Author Contributions:** Conceptualization, N.W.; methodology, N.W.; software, N.W.; validation, N.W.; formal analysis, N.W.; investigation, N.W.; resources, N.W.; data curation, N.W. and Y.W.; writing—original draft preparation, N.W. and Y.W.; writing—review and editing, N.W. and Y.W.; visualization, N.W. and Y.W. All authors have read and agreed to the published version of the manuscript.

**Funding:** This research was funded by the National Natural Science Foundation of China (Grant No.: 11804021), Chinese Postdoctoral Science Foundation (Grant No.: 2017M620604), and the Fundamental Research Funds for the Central Universities, China (Grant No.: FRF-TP-16-080A1). The APC was funded by Chinese Postdoctoral Science Foundation (Grant No.: 2017M620604).

**Data Availability Statement:** The original contributions presented in the study are included in the article, further inquiries can be directed to the corresponding author.

**Conflicts of Interest:** The authors declare no conflict of interest.

#### References

1. Jeon, N.J.; Na, H.; Jung, E.H.; Yang, T.-Y.; Lee, Y.G.; Kim, G.; Shin, H.-W.; Seok, S.I.; Lee, J.; Seo, J. A fluorene-terminated hole-transporting material for highly efficient and stable perovskite solar cells. *Nat. Energy* **2018**, *3*, 682–689. [[CrossRef](#)]
2. Yang, W.S.; Park, B.-W.; Jung, E.H.; Jeon, N.J.; Kim, Y.C.; Lee, D.U.; Shin, S.S.; Seo, J.; Kim, E.K.; Noh, J.H.; et al. Iodide management in formamidinium-lead-halide-based perovskite layers for efficient solar cells. *Science* **2017**, *356*, 1376–1379. [[CrossRef](#)]

3. Saliba, M.; Matsui, T.; Seo, J.-Y.; Domanski, K.; Correa-Baena, J.-P.; Nazeeruddin, M.K.; Zakeeruddin, S.M.; Tress, W.; Abate, A.; Hagfeldt, A.; et al. Cesium-containing triple cation perovskite solar cells: Improved stability, reproducibility and high efficiency. *Energy Environ. Sci.* **2016**, *9*, 1989–1997. [[CrossRef](#)]
4. Lee, J.; Kim, D.; Kim, H.; Seo, S.; Cho, S.M.; Park, N. Formamidinium and Cesium Hybridization for Photo- and Moisture-Stable Perovskite Solar Cell. *Adv. Energy Mater.* **2015**, *5*, 1501310. [[CrossRef](#)]
5. Bi, D.; Tress, W.; Dar, M.I.; Gao, P.; Luo, J.; Renevier, C.; Schenk, K.; Abate, A.; Giordano, F.; Baena, J.-P.C.; et al. Efficient luminescent solar cells based on tailored mixed-cation perovskites. *Sci. Adv.* **2016**, *2*, e1501170. [[CrossRef](#)] [[PubMed](#)]
6. Kojima, A.; Teshima, K.; Shirai, Y.; Miyasaka, T. Organometal Halide Perovskites as Visible-Light Sensitizers for Photovoltaic Cells. *J. Am. Chem. Soc.* **2009**, *131*, 6050–6051. [[CrossRef](#)] [[PubMed](#)]
7. Conings, B.; Drijkoningen, J.; Gauquelin, N.; Babayigit, A.; D’Haen, J.; D’Olieslaeger, L.; Ethirajan, A.; Verbeeck, J.; Manca, J.; Mosconi, E.; et al. Intrinsic Thermal Instability of Methylammonium Lead Trihalide Perovskite. *Adv. Energy Mater.* **2015**, *5*, 1500477. [[CrossRef](#)]
8. Nagabhushana, G.P.; Shivaramaiah, R.; Navrotsky, A. Direct calorimetric verification of thermodynamic instability of lead halide hybrid perovskites. *Proc. Natl. Acad. Sci. USA* **2016**, *113*, 7717–7721. [[CrossRef](#)] [[PubMed](#)]
9. Yi, C.; Luo, J.; Meloni, S.; Boziki, A.; Ashari-Astani, N.; Grätzel, C.; Zakeeruddin, S.M.; Röthlisberger, U.; Grätzel, M. Entropic stabilization of mixed A-cation ABX<sub>3</sub> metal halide perovskites for high performance perovskite solar cells. *Energy Environ. Sci.* **2015**, *9*, 656–662. [[CrossRef](#)]
10. Colella, S.; Mosconi, E.; Fedeli, P.; Listorti, A.; Gazza, F.; Orlandi, F.; Ferro, P.; Besagni, T.; Rizzo, A.; Calestani, G.; et al. MAPbI<sub>3-x</sub>Cl<sub>x</sub> Mixed Halide Perovskite for Hybrid Solar Cells: The Role of Chloride as Dopant on the Transport and Structural Properties. *Chem. Mater.* **2013**, *25*, 4613–4618. [[CrossRef](#)]
11. Saliba, M.; Matsui, T.; Domanski, K.; Seo, J.-Y.; Ummadisingu, A.; Zakeeruddin, S.M.; Correa-Baena, J.-P.; Tress, W.R.; Abate, A.; Hagfeldt, A.; et al. Incorporation of rubidium cations into perovskite solar cells improves photovoltaic performance. *Science* **2016**, *354*, 206–209. [[CrossRef](#)] [[PubMed](#)]
12. Ahmad, W.; Khan, J.; Niu, G.; Tang, J. Inorganic CsPbI<sub>3</sub> Perovskite-Based Solar Cells: A Choice for a Tandem Device. *Sol. RRL* **2017**, *1*, 1700048. [[CrossRef](#)]
13. Eperon, G.E.; Paterno, G.M.; Sutton, R.J.; Zampetti, A.; Haghighirad, A.A.; Cacialli, F.; Snaith, H.J. Inorganic caesium lead iodide perovskite solar cells. *J. Mater. Chem. A* **2015**, *3*, 19688–19695. [[CrossRef](#)]
14. Zhou, W.; Zhao, Y.; Zhou, X.; Fu, R.; Li, Q.; Zhao, Y.; Liu, K.; Yu, D.; Zhao, Q. Light-Independent Ionic Transport in Inorganic Perovskite and Ultrastable Cs-Based Perovskite Solar Cells. *J. Phys. Chem. Lett.* **2017**, *8*, 4122–4128. [[CrossRef](#)]
15. Chen, C.; Lin, H.; Chiang, K.; Tsai, W.; Huang, Y.; Tsao, C.; Lin, H. All-Vacuum-Deposited Stoichiometrically Balanced Inorganic Cesium Lead Halide Perovskite Solar Cells with Stabilized Efficiency Exceeding 11%. *Adv. Mater.* **2017**, *29*, 1605290. [[CrossRef](#)]
16. Dastidar, S.; Hawley, C.J.; Dillon, A.D.; Gutierrez-Perez, A.D.; Spanier, J.E.; Fafarman, A.T. Quantitative Phase-Change Thermodynamics and Metastability of Perovskite-Phase Cesium Lead Iodide. *J. Phys. Chem. Lett.* **2017**, *8*, 1278–1282. [[CrossRef](#)]
17. Frolova, L.A.; Anokhin, D.V.; Piriyazev, A.A.; Luchkin, S.Y.; Dremova, N.N.; Stevenson, K.J.; Troshin, P.A. Highly Efficient All-Inorganic Planar Heterojunction Perovskite Solar Cells Produced by Thermal Coevaporation of CsI and PbI<sub>2</sub>. *J. Phys. Chem. Lett.* **2016**, *8*, 67–72. [[CrossRef](#)]
18. Kim, Y.G.; Kim, T.-Y.; Oh, J.H.; Choi, K.S.; Kim, Y.-J.; Kim, S.Y. Cesium lead iodide solar cells controlled by annealing temperature. *Phys. Chem. Chem. Phys.* **2017**, *19*, 6257–6263. [[CrossRef](#)]
19. Brgoch, J.; Lehner, A.J.; Chabinyk, M.; Seshadri, R. Ab Initio Calculations of Band Gaps and Absolute Band Positions of Polymorphs of RbPbI<sub>3</sub> and CsPbI<sub>3</sub>: Implications for Main-Group Halide Perovskite Photovoltaics. *J. Phys. Chem. C* **2014**, *118*, 27721–27727. [[CrossRef](#)]
20. Eaton, S.W.; Lai, M.; Gibson, N.A.; Wong, A.B.; Dou, L.; Ma, J.; Wang, L.-W.; Leone, S.R.; Yang, P. Lasing in robust cesium lead halide perovskite nanowires. *Proc. Natl. Acad. Sci. USA* **2016**, *113*, 1993–1998. [[CrossRef](#)]
21. Trots, D.; Myagkota, S. High-temperature structural evolution of caesium and rubidium triiodoplumbates. *J. Phys. Chem. Solids* **2008**, *69*, 2520–2526. [[CrossRef](#)]
22. Stoumpos, C.C.; Mao, L.; Malliakas, C.D.; Kanatzidis, M.G. Structure–Band Gap Relationships in Hexagonal Polytypes and Low-Dimensional Structures of Hybrid Tin Iodide Perovskites. *Inorg. Chem.* **2016**, *56*, 56–73. [[CrossRef](#)]
23. Lin, J.; Lai, M.; Dou, L.; Kley, C.S.; Chen, H.; Peng, F.; Sun, J.; Lu, D.; Hawks, S.A.; Xie, C.; et al. Thermochromic halide perovskite solar cells. *Nat. Mater.* **2018**, *17*, 261–267. [[CrossRef](#)]
24. Zhao, X.-G.; Dalpian, G.M.; Wang, Z.; Zunger, A. Polymorphous nature of cubic halide perovskites. *Phys. Rev. B* **2020**, *101*, 155137. [[CrossRef](#)]
25. Yang, R.X.; Tan, L.Z. First-Principles Characterization of Surface Phonons of Halide Perovskite CsPbI<sub>3</sub> and Their Role in Stabilization. *J. Phys. Chem. Lett.* **2021**, *12*, 9253–9261. [[CrossRef](#)]
26. Kye, Y.-H.; Yu, C.-J.; Jong, U.-G.; Ri, K.-C.; Kim, J.-S.; Choe, S.-H.; Hong, S.-N.; Li, S.; Wilson, J.N.; Walsh, A. Vacancy-Driven Stabilization of the Cubic Perovskite Polymorph of CsPbI<sub>3</sub>. *J. Phys. Chem. C* **2019**, *123*, 9735–9744. [[CrossRef](#)]
27. Jiang, C.; Wang, Y.; Zhou, R.; Wang, H.; Chen, Q. Air molecules in XPbI<sub>3</sub> (X = MA, FA, Cs) perovskite: A degradation mechanism based on first-principles calculations. *J. Appl. Phys.* **2018**, *124*, 085105. [[CrossRef](#)]
28. Li, W.; Liu, P.; Wang, F.; Pan, L.; Guo, H.; Chen, Y.; Yang, S.-E. Phase stability and impact of water on CsSnI<sub>3</sub> perovskite. *Appl. Phys. Express* **2020**, *13*, 071003. [[CrossRef](#)]

29. Kresse, G.; Joubert, D. From ultrasoft pseudopotentials to the projector augmented-wave method. *Phys. Rev. B* **1999**, *59*, 1758–1775. [[CrossRef](#)]
30. Kohn, W.; Sham, L.J. Self-consistent equations including exchange and correlation effects. *Phys. Rev.* **1965**, *140*, A1133–A1138. [[CrossRef](#)]
31. Perdew, J.P.; Burke, K.; Ernzerhof, M. Generalized gradient approximation made simple. *Phys. Rev. Lett.* **1996**, *77*, 3865–3868. [[CrossRef](#)]
32. Huang, Y.; Yin, W.-J.; He, Y. Intrinsic Point Defects in Inorganic Cesium Lead Iodide Perovskite CsPbI<sub>3</sub>. *J. Phys. Chem. C* **2018**, *122*, 1345–1350. [[CrossRef](#)]
33. Li, Y.; Zhang, C.; Zhang, X.; Huang, D.; Shen, Q.; Cheng, Y.; Huang, W. Intrinsic point defects in inorganic perovskite CsPbI<sub>3</sub> from first-principles prediction. *Appl. Phys. Lett.* **2017**, *111*, 162106. [[CrossRef](#)]
34. Yang, K.; Zhang, Y.; Lu, H. First-principles study on the geometric, electronic and thermodynamic properties of the CsPbI<sub>3</sub> (001) surfaces. *IOP Conf. Ser. Earth Environ. Sci.* **2021**, *692*, 022020. [[CrossRef](#)]
35. Grimme, S.; Antony, J.; Ehrlich, S.; Krieg, H. A consistent and accurate ab initio parametrization of density functional dispersion correction (DFT-D) for the 94 elements H-Pu. *J. Chem. Phys.* **2010**, *132*, 154104. [[CrossRef](#)] [[PubMed](#)]
36. Steiner, S.; Khmelevskiy, S.; Marsmann, M.; Kresse, G. Calculation of the magnetic anisotropy with projected-augmented-wave methodology and the case study of disordered Fe<sub>1-x</sub>Cox alloys. *Phys. Rev. B* **2016**, *93*, 224425. [[CrossRef](#)]
37. Shishkin, M.; Kresse, G. Self-consistent \$GW\$ calculations for semiconductors and insulators. *Phys. Rev. B* **2007**, *75*, 235102. [[CrossRef](#)]
38. Chen, G.-Y.; Guo, Z.-D.; Gong, X.-G.; Yin, W.-J. Kinetic pathway of  $\gamma$ -to- $\delta$  phase transition in CsPbI<sub>3</sub>. *Chem* **2022**, *8*, 3120–3129. [[CrossRef](#)]
39. Wang, N.; West, D.; Liu, J.; Li, J.; Yan, Q.; Gu, B.-L.; Zhang, S.B.; Duan, W. Microscopic origin of the p-type conductivity of the topological crystalline insulator SnTe and the effect of Pb alloying. *Phys. Rev. B* **2014**, *89*, 045142. [[CrossRef](#)]
40. Wang, N.; Wu, Y. Intrinsic defects on  $\alpha$ ,  $\gamma$  and  $\delta$ -CsPbI<sub>3</sub> (001) surfaces and implications for the  $\alpha/\gamma$  to  $\delta$  phase transition. *Phys. Chem. Chem. Phys.* **2023**, *25*, 16077–16085. [[CrossRef](#)]
41. Mosquera-Lois, I.; Kavanagh, S.R.; Klarbring, J.; Tolborg, K.; Walsh, A. Imperfections are not 0 K: Free energy of point defects in crystals. *Chem. Soc. Rev.* **2023**, *52*, 5812–5826. [[CrossRef](#)]
42. Zunger, A.; Malyi, O.I. Understanding Doping of Quantum Materials. *Chem. Rev.* **2021**, *121*, 3031–3060. [[CrossRef](#)]
43. Wei, S.-H.; Zhang, S.B. Chemical trends of defect formation and doping limit in II-VI semiconductors: The case of CdTe. *Phys. Rev. B* **2002**, *66*, 155211. [[CrossRef](#)]
44. Van de Walle, C.G.; Neugebauer, J. First-principles calculations for defects and impurities: Applications to III-nitrides. *J. Appl. Phys.* **2004**, *95*, 3851–3879. [[CrossRef](#)]
45. Freysoldt, C.; Grabowski, B.; Hickel, T.; Neugebauer, J.; Kresse, G.; Janotti, A.; Van de Walle, C.G. First-principles calculations for point defects in solids. *Rev. Mod. Phys.* **2014**, *86*, 253–305. [[CrossRef](#)]
46. Makov, G.; Payne, M.C. Periodic boundary conditions in ab initio calculations. *Phys. Rev. B* **1995**, *51*, 4014–4022. [[CrossRef](#)] [[PubMed](#)]
47. Afsari, M.; Boochani, A.; Hantezadeh, M. Electronic, optical and elastic properties of cubic perovskite CsPbI<sub>3</sub>: Using first principles study. *Optik* **2016**, *127*, 11433–11443. [[CrossRef](#)]
48. Hellström, M.; Spångberg, D.; Hermansson, K.; Broqvist, P. Band-Filling Correction Method for Accurate Adsorption Energy Calculations: A Cu/ZnO Case Study. *J. Chem. Theory Comput.* **2013**, *9*, 4673–4678. [[CrossRef](#)] [[PubMed](#)]
49. Zhao, X.-G.; Wang, Z.; Malyi, O.I.; Zunger, A. Effect of static local distortions vs. dynamic motions on the stability and band gaps of cubic oxide and halide perovskites. *Mater. Today* **2021**, *49*, 107–122. [[CrossRef](#)]

**Disclaimer/Publisher's Note:** The statements, opinions and data contained in all publications are solely those of the individual author(s) and contributor(s) and not of MDPI and/or the editor(s). MDPI and/or the editor(s) disclaim responsibility for any injury to people or property resulting from any ideas, methods, instructions or products referred to in the content.